CHEMICAL ENGINEERING TRANSACTIONS
VOL. 74, 2019
A publication of AIDIC
The Italian Association of Chemical Engineering
Online at www.cetjournal.it
Guest Editors: Sauro Pierucci, Jiří Jaromír Klemeš, Laura Piazza

ISBN 978-88-95608-71-6; **ISSN** 2283-9216
DOI: 10.3303/CET1974071

CFD Modelling of the Evaporation of Biphasic (Solid-Liquid) Individual Droplets in a Spray Dryer

Daniel Sebastia-Saez[a,*], Francisco M. Baena-Moreno[b], Harvey Arellano-Garcia[a,c]

[a]Department of Chemical and Process Engineering, University of Surrey, GU2 7XH Guildford, United Kingdom
[b]Department of Chemical and Environmental Engineering, University of Seville, 41092 Seville, Spain
[c]Prozess- und Anlagentechnik, Brandenburgische Technische Universität Cottbus-Senftenberg, D-03046 Cottbus, Germany
j.sebastiasaez@surrey.ac.uk

An analysis of the literature shows the capability of Computational Fluid Dynamics to represent the hydrodynamics and heat transfer within spray dryers, as well as the prediction of droplet collision, agglomeration and wall deposition. The literature also reveals that no model published so far describes the drying of individual droplets, the study of which is restricted to experimental methods such as ultrasonic levitation. This article presents an Euler-Lagrange three-phase numerical set-up to simulate the drying of individual droplets within a spray dryer. The defining parameters of both phases, i.e. air and the biphasic (solid-liquid) droplets are taken from a barbotine slurry used for ceramic tile production. A single droplet size has been used—the characteristic Rosin-Rammler droplet size from the distribution generated by an actual spray injector published previously in the literature. The model predicts the theoretical linear evolution of the square diameter according to the D^2-law, and the temperature and mass exchange with the environment. This unique numerical set-up allows calculating the Stokes number associated with a given trajectory path as well, providing designers with an accurate degree of control over the fate of individual droplets. The proposed model is therefore a powerful tool intended to support the design and optimization of industrial spray dryers.

1. Introduction

Spray dryers constitute a basic unit operation in food industry (Kuriakose and Anandharamakrishnan, 2010; Zondervan et al., 2015), pharmaceutical (Poozesh et al., 2018), detergents, agrochemicals, carbon capture (Kavoshi et al., 2015), high value particles for medical applications (Golman and Julklang, 2014), et cetera. Spray drying is nonetheless, a basic unit operation in ceramic tile production, an industry of crucial importance for the Italian economy.

Computational Fluid Dynamics (CFD) models reported in the literature show maps of temperature, velocities and humidity, as well of the trajectories of spray droplets within the dryer. Other models have been devoted to the prediction of particle collision, agglomeration, and wall deposition; which are of crucial importance in industry, for they affect directly the quality of the final product, as well as being an indicator of potential malfunction (Mezhericher et al., 2010). In this line, Jaskulski et al. (2018) presented a CFD set-up where external collision and droplet agglomeration models were fed into in order to predict the probability of occurrence of such phenomena. Wall deposition in spray dryers using CFD was investigated by Ali et al. (2015), who presented a drying detergent slurry CFD simulation the output of which was the probability of particle deposition against the walls. The authors obtained numerically-calculated humidity, temperature and discrete phase concentration maps, and inferred the probability of particle deposition. Other articles do not analyse the troubleshooting and design capabilities of CFD in the field of spray drying, but focus on analysing the suitability of current numerical methods. Being the flow inside a spray dryer extremely chaotic (particularly in the case of counter-current configurations), Jubaer et al. (2019) have discussed the application of currently developed turbulence models to describe the flow within spray dryers; and Langrish et al. (2004) studied the effect of induced swirl on the functioning of the dryer.

All the models consulted lack however, the capability of analysing the fate of individual droplets within a spray dryer, along with the change in diameter according to the well-established D^2-law, which so far has been

Paper Received: 2 July 2018; Revised: 10 October 2018; Accepted: 2 February 2019

Please cite this article as: Sebastia-Saez D., Baena-Moreno F.M., Arellano-Garcia H., 2019, CFD Modelling of the Evaporation of Biphasic (solid-liquid) Individual Droplets in a Spray Dryer, Chemical Engineering Transactions, 74, 421-426 DOI:10.3303/CET1974071

proved by means of experimental work such as using the method of ultrasonic levitation (Kreimer et al., 2018). The model presented herein tries to fill this gap and presents a unique set-up in order to track the fate of individual droplets within the spray dryer. The user of the model presented herein can therefore, track the change in diameter and temperature associated with the trajectory of the droplet, and thus determine the exact instant when drying out occurs.

2. Methods

A three-phase simulation set-up was developed using the commercial CFD software ANSYS CFX v19.1. The set-up was run in a PC with four CPUs in parallel. The numerical domain consisted of a 2D representation of the spray dryer located at the Ceramic Technology Institute of Castelló (Spain). The link between the actual spray dryer and the 2D numerical domain is represented in Figure 1, which also includes the mesh used and the structure of the jet produced by the nozzle. The use of a 2D numerical domain responds to computational limitations, which made the complete representation of the dryer unfeasible. The interesting part of the simulation set-up presented herein, however, was the visualization of the droplet trajectories and the change in diameter of the droplets according to the D^2-law; both characteristics were reproduced using the 2D set-up.

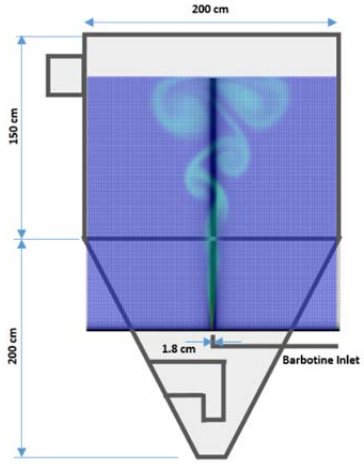

Figure 1: Schematic drawing of the spray dryer and the 2D numerical domain used to obtain the results of this work.

The 2D structured mesh was comprised of 35,600 nodes (200 nodes in the vertical direction and 178 in the horizontal direction, with the minimum distance between nodes being 500 μm). ANSYS ICEM blocking strategy was used to develop the mesh. The simulation follows a three-phase Euler-Lagrange approach, with the continuous phase, i.e. the air of the spray, defined as a mixture of dry air and water vapor, with a temperature at inlet conditions of 900°C and no initial water vapor concentration. The velocity profile of the jet obtained by means of Laser Doppler Anemometry at a vertical distance of 2.5 mm from the nozzle was introduced as the boundary condition for the spray inlet; whereas the Rosin-Rammler diameter corresponding to the droplet size distribution generated by the nozzle was obtained by way of Laser Diffractometry and subsequently introduced in the simulation set-up as well (Sebastia-Saez et al., 2019). The discrete phase (barbotine) is defined as an ideal mixture of liquid water and kaolinite $Al_2Si_2O_5(OH)_4$ (density of 2650 kg/m^3 and a specific heat capacity of 750 J/kg/K). The initial mass fraction of the water and kaolinite in the droplets as they enter the domain were 0.4/0.6, respectively. A mass flow rate of 0.0014 kg/s according to a cone with an opening angle of 34° was set at the Lagrangian phase inlet, at ambient temperature (25°C). Non-slip boundary conditions were set on either wall of the domain. Openings were set on the rest of the domain boundaries. The calculations were carried out in transient regime with a time step of 0.01 s and up to 4.5 s flow time, which was enough to see the drying of the droplets. The maximum number of iterations per time step allowed to reach convergence was 10. The k-ε model was selected to close the Navier-Stokes system. Particle collision, coalescence and secondary breakup were omitted. Fully coupled momentum exchange between the continuous and the discrete phase was selected, which allows for a more realistic representation of the droplet trajectories within the dryer. The Ranz-Marshall model was the option selected to describe heat transfer.

3. Results and discussion

The novelty of this model lies therefore on the implementation of the D^2-law in a CFD simulation. The D^2-law establishes that, upon evaporation, the square diameter of a droplet decreases following a linear trend according to

$$D^2(t) = D_0^2 - \beta t, \tag{1}$$

where D^2 [m^2] is the square diameter of the droplet in (with the subscript 0 denoting the initial value), t [s] is time, and β [m^2/s] is the evaporation rate (Faeth, 1977; Law, 1982) calculated as

$$\beta = 8\frac{\rho_g}{\rho_d}\mathcal{D}_g \ln(1 + B_M), \tag{2}$$

where $\mathcal{D}_g$ [m^2/s] is the diffusion coefficient of the component being evaporated into the surrounding continuous phase, ρ_g [kg/m^3] is the density of the surrounding gas phase, ρ_d [kg/m^3] is the density of the droplet, and B_M is the dimensionless Spalding mass transfer coefficient.

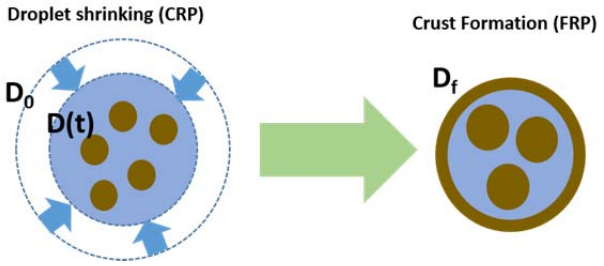

Figure 2: Schematic illustration of the D^2-law and the formation of a solid crust on the surface of the droplet, which hinders evaporation mass transfer towards the environment.

As for the case of biphasic (solid-liquid) droplets, the linear decrease in square diameter occurs until the formation of a solid crust, past-which the loss of liquid component encounters the resistance posed by the porosity of the solid crust, resulting in a nearly constant square diameter. The drying process is thus, divided in two stages, namely the Constant Rate Period (CRP) and the Falling Rate Period (FRP) (Al Zaitone, 2009). A schematic of the process has been included in Figure 2. The CRP is represented on the left-hand side, where the droplet shrinks (with a diameter $D(t)$ which is a function of time) from an initial diameter D_0. Extensive experimental work has been carried out on the drying of single droplets (Yarin et al., 2002; Brenn et al., 2007; Al Zaitone and Tropea, 2011). Important conclusions may be drawn from the study of droplet evaporation using either the acoustic levitation or the glass filament method, but these methods do not provide information as to how droplet evaporation occurs upon the complex conditions encountered within a spray dryer. The simulation set-up herein aims at providing an answer to the latter issue. For instance, it can be used to shed light on how the evaporation rate β changes as the droplet crosses areas of the dryer with varying velocities and temperatures.

To that purpose, the blue data series in Figure 3a (marked as particle velocity in the legend) shows the evolution of the velocity of a droplet following a trajectory within the domain. The velocity of the continuous Eulerian phase (air) on the same trajectory (red data series), and the difference in velocity between both the continuous and the discrete phase (black data series) are represented as well with their respective data series. The trajectory taken for this analysis is depicted in the inset plot in Figure 3a, where the boundaries of the computational domain are represented by a thin full line in order to provide the reader with an idea of the distance travelled by the droplet following that trajectory (the domain has dimensions 2 × 2 m). One can appreciate in the inset plot that the trajectory of the droplet begins at the centre line of the domain, where the injection nozzle is placed, and travels upwards approximately 1.2 m before experiencing a turning point after which the droplet begins to fall. The data series corresponding to air shows that the velocity damps to an average value of approximately 2 m/s short after injection into the domain (the latter occurring at an average of 14 m/s). The velocity of the droplet, which is injected into the domain at 14 m/s decreases following a nearly linear decreasing trend caused by gravity and the drag induced by the surrounding continuous phase, i.e. fully coupled momentum exchange has been selected in the simulation set-up. One can see, therefore, that during the upwards part, the droplet follows its trajectory detached from the flow it is within, given the difference between the gas and the particle velocities. The portion of the three data series corresponding to either the upwards and the downwards part of the trajectory are separated in Figure 3a by a blue vertical dashed line

(the left-hand side corresponds to the upwards part, and the right-hand side to the downwards part). From the portion of the data series corresponding to the downwards part, one can see that there is still some degree of detachment between the droplet and the surrounding continuous phase as the difference in velocity between both the continuous and the discreet phases presents three peaks. The absolute velocity of the droplet (blue series) presents a nearly constant value, which suggests that it has reached its terminal velocity at about 2 m/s. In accordance to the velocities discussed up to this point, Figure 3b shows the evolution of the Stokes number associated with the trajectory considered in this study. The dimensionless Stokes number Stk, which indicates whether a particle follows the fluid streamlines, is calculated as

$$Stk = \frac{t_0\, u}{l}, \tag{3}$$

where u [m/s] is the velocity of the fluid main stream, and l [m] is the characteristic length, which in this case equals the diameter of the droplet. The droplet relaxation time is denoted by t_0 [s], and is calculated as $t_0 = \frac{\rho_d D^2}{18\mu_g}$, being ρ_d [kg/m^3] the density of the droplet, D^2 [m^2] the square diameter of the droplet, and μ_g[Pa·s] the dynamic viscosity of the continuous phase. To calculate the relaxation time, the evolution of the average density of the droplet as the liquid component evaporates, as well as the evolution of the square diameter along the trajectory have been considered instead of a constant value. To complete the calculation of the Stokes number, the velocity of the gas phase along the same trajectory has been used. Figure 3b shows again an almost linear decay of the Stokes number which decreases from around Stk=10,000 to approximately 4 at the turning point, where the vertical component of the droplet velocity is zero. Indeed, this minimum in the relative velocity of the droplet with respect to the continuous phase does not indicate that the droplet is carried by the continuous phase, but the turning point in its trajectory. The minima and maxima found afterwards, however, do suggest some degree of interplay between attachment and detachment of the droplet from the continuous phase. The values shown in the inset plot of Figure 3b help reinforce the fact that the droplet travels detached from the continuous phase for most of its trajectory, as Stk>20 for most of the particle travelling time.

Further evidence that the droplet is generally not carried away (detached) by the continuous phase can be found in the two vector plots in Figure 4, which show the formation of eddies near the trajectory turning point (upper vector plot) and on the downwards part of the trajectory (lower vector plot). In both cases, one can observe that the direction of the vectors and the droplet travel on opposite directions on the downwards portion of the trajectory (when the Stokes number Stk is lowest).

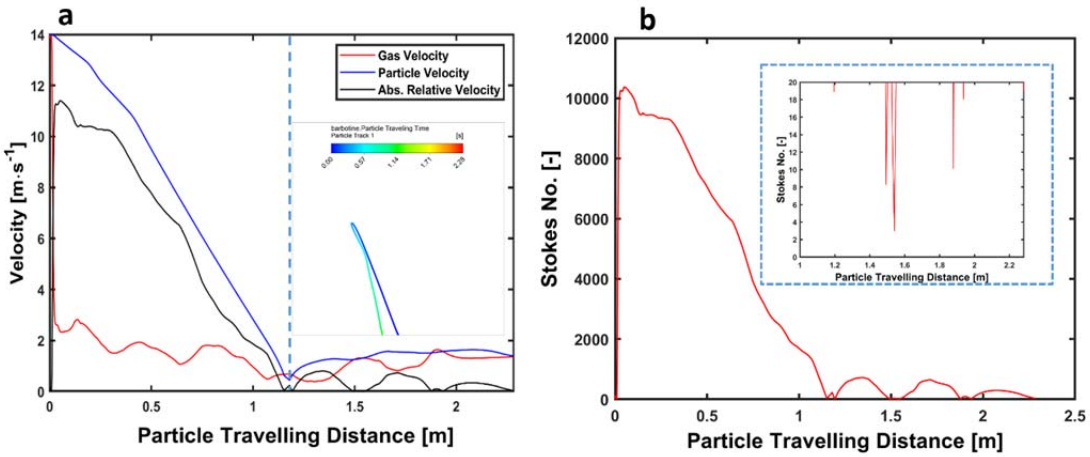

Figure 3: a) Plots of velocity (along the trajectory depicted in the inset plot), and b) Evolution of the Stokes number Stk along the same trajectory.

One can therefore find two separate stages in the hydrodynamic behaviour of the droplet, which affect the evaporation rate as depicted in Figure 5. Figure 5a expresses the results expected according to the D^2-law), that is, a first stage where a linear decrease of the square diameter occurs (the FRP), followed by another stage (the CRP) where the diameter of the droplet is kept constant (after depletion of the liquid component

and subsequent formation of an external solid crust). The same square diameter data are expressed in Figure 5b, but with respect to particle travel distance instead, in order to correlate the specifics described in Figure 3 and 4 with the evolution of the square diameter. The point at which the trajectory turning point occurs is marked on the graph, clearly separating two different evaporation rates. In conclusion, the flow regime as a function has a clear effect on the evaporation rate β, and thus on the drying-up time of the droplet. It is worth saying that in reality water continues to evaporate from the droplet after the formation of the solid crust, although considerably hindered by it. In this model, however, the square diameter is kept constant when depletion of the liquid component (in this case water) occurs (see Sebastia-Saez et al., 2019 for further detail on the time evolution of both the solid and liquid components of the droplet, and for experimental validation of the velocity field generated by the nozzle).

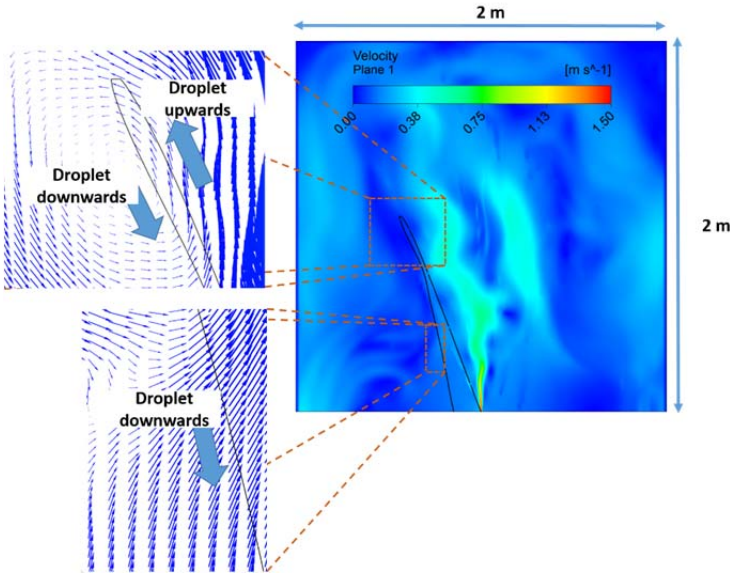

Figure 4: Trajectory of the droplet considered in this study in a velocity map of the jet. Two inset vector plots indicate the detachment of the droplet from the eddies formed in the continuous phase.

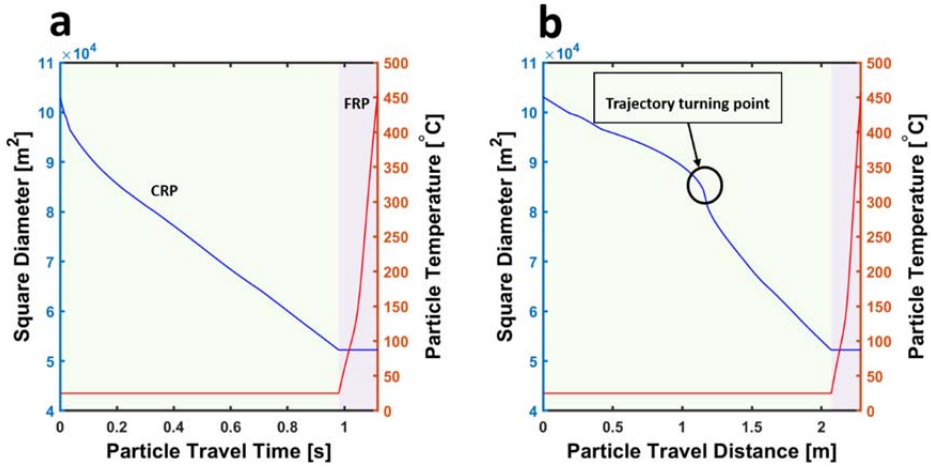

Figure 5: Evolution of the droplet square diameter with respect to particle travel time (a), and particle travel distance (b).

4. Conclusions

A three-phase numerical model of the hydrodynamics, heat and mass transfer characteristics of an industrial spray dryer is presented here. The results analyze the fate of an individual droplet following one of the trajectories within the dryer. The model allows gaining detailed information on the time evolution of the droplet hydrodynamics and temperature. This allows establishing the instant and location where the droplet dries out.

In this line, the Stokes number associated with the droplet following the trajectory studied has been obtained. For a droplet with an initial diameter of 321 μm, the calculations show a Stokes number far greater than one for the upwards part of the trajectory (which indicates that the droplet does not closely follow the streamlines defined by the continuous phase) followed by a downwards part where the droplet is carried by the continuous phase at some degree. A difference between the evaporation rates in both stages is patent from the results of the evolution of the square diameter with the particle travel distance.
This model proves as an important tool to gain insight on phenomena taking place within an industrial dryer, otherwise difficult to gain by using only experimental methods. The model is thus, valuable to assist with the design and dimensioning of spray dryers.

Acknowledgments

The authors gratefully acknowledge the Ceramic Technology Institute in Castelló (Spain), and Universitat Jaume I (Spain).

References

Ali M., Mahmud T., Heggs P.J., Ghadiri M., Bayly A., Ahmadian H., Martin de Juan L., CFD simulation of a counter-current spray drying tower with stochastic treatment of particle-wall collision, Procedia Engineering, 102, 1284–1294.

Al Zaitone B.A., Tropea C., 2011, Evaporation of pure liquid droplets: Comparison of droplet evaporation in an acoustic field versus glass-filament, Chem. Eng. Sci., 66, 3914–3921.

Al Zaitone B.A., 2009, Drying of multiphase single droplets in ultrasonic levitator, PhD Thesis, University of Technischen Universität Darmstadt, Darmstadt, Germany.

Brenn G., Deviprasath L.J., Durst F., Fink C., 2007, Evaporation of acoustically levitated multi-component liquid droplets, Int. J. Heat Mass Tran., 50, 5073–5086.

Golman, B., Julklang, W., 2014, Study on spray drying for the production of high-value particles. Chem. Engineer. Trans., 39, 997–1002.

Faeth, G. M., 1977, Current status of droplet and liquid combustion. Prog. Energ. Combust., 3, 191–224.

Jaskulski M., Wawrzyniak, P., Zbiciński I., 2018, CFD simulations of droplet and particle agglomeration in an industrial counter-current spray dryer, Adv. Powder Technol., 29, 1724–1733.

Jubaer H., Afshar S., Xiao J., Chen X.D., Selomulya C., Woo M.W., 2019, On the effect of turbulence models on CFD simulations of a counter-current spray drying models, Chem. Eng. Res. Des., 141, 592–607.

Kavoshi L., Rahimi A., Hatamipour M.S., 2015, CFD modelling and experimental study of carbon dioxide removal in a lab-scale spray dryer, Chem. Eng. Res. Des., 98, 157–167.

Kreimer M., Aigner I., Sacher S., Krumme M., Mannschott T., van der Wel P., Kaptein A., Schroettner H., Brenn G., Khinast J.G., 2018, Mechanical strength of microspheres produced by drying of acoustically levitated suspension droplets, Powder Technol., 325, 247–260.

Kuriakose R., Anandharamakrishnan, C., 2010, Computational fluid dynamics (CFD) applications in spray drying of food products, Trends Food Sci. Tech., 21, 383–398.

Langrish T.A.G., Williams J., Fletcher D.F., 2004, Simulation of the effects of inlet swirl on gas flow patterns in a pilot-scale spray dryer, Chem. Eng. Res. Des., 82, 821–833.

Law C. K., 1982, Recent advances in droplet vaporisation and combustion. Prog. Energ. Combust., 8, 171–201.

Mezhericher M., Levy A., Borde I., 2010, Spray drying modelling based on advanced droplet drying kinetics, Chem. Eng. Process.: Process Intensification, 49, 1205–1213.

Poozesh S., Lu K., Marsac P.J., 2018, On the particle formation in spray drying process for bio-pharmaceutical applications: Interrogating a new model via Computational Fluid Dynamics, Int. J. Heat Mass Tran., 122, 863–876.

Sebastia-Saez D., Hernandez L., Arellano-Garcia H., Julia J.E., 2019, Numerical and experimental characterization of the hydrodynamics and drying kinetics of a barbotine slurry spray, Chem. Eng. Sci., 195, 83–94.

Yarin A.L., Brenn G., Rensink D., 2002, Evaporation of acoustically levitated droplets of binary liquid mixtures, Int. J. Heat Fluid Fl., 23, 471–486.

Zondervan E., Monsanto M., Meuldijk J., 2015, Product driven process synthesis for the recovery of vitality ingredients from plant materials, Chem. Engineer. Trans., 43, 61–66